

Mean current in Ps/Spd MultiAnode PhotoMultipliers Tubes

*E. Aguilo, R. Ballabriga, M. Calvo, Ll. Garrido, D. Gascon, R. Graciani,
S. Luengo, J. Riera, M. Rosello, X. Vilasis-Cardona*

Universitat de Barcelona, ECM departement

E-08028 Diagonal 647 (Barcelona)

IFAE, Universitat Autònoma de Barcelona

E-8193 Bellaterra (Barcelona)

*G. Bohner, R. Bonnefoy, C. Carloganu, R. Cornat, M. Crouau, O. Deschamps,
S. Monteil, J. Lecoq, R. Lefèvre, P. Perret*

Laboratoire de Physique Corpusculaire, Clermont-Ferrand

Université Blaise Pascal / CNRS-IN2P3

F-63177 Aubière Cedex, France

1 Introduction

Multi-Anode PhotoMultiplier Tubes (MA-PMT) are so far the best candidates for the read-out of the scintillator light of both the SPD and PS detectors. The basic characteristics of 64 anodes PMT from the Hamamatsu company were considered to support the designs of the VFE electronics for these two detectors. These MA-PMTs are provided with a specific base by the constructor.

In a recent period, the choice of the MA-PMT base, which defines the way the interdynodes voltages are set, has been scrutinized. In that respect, a key parameter of the correct behaviour of the MA-PMT is the average anode current. This quantity has been estimated in the present design of the VFE electronics, from the energy deposits in the detector with simulated events for all the anodes of all the MA-PMT, symmetrically for SPD and PS.

The results of these computations revealed two main issues : the first one is that the average anode currents for some MA-PMT are beyond the specifications of the constructor, requiring minimally the design of a dedicated base. The second one, far more critical, concerns the ageing of the photodetector. Dedicated studies showed that the gain of the MA-PMT in the condition of large average anode current is rapidly decreased.

The first section of the note is dedicated to the estimate of the average anode current from the energy deposits in the LHCb SPD and preshower. The particles which actually deposit the energy have been traced back. The second section summarises the first ageing results of the test bench specially set up in Clermont-Ferrand. The third part of this document describes the immediate actions which are underway and the perspectives that have been considered so far in terms of the choice of the MA-PMT and the possible redesigns of the electronics for the Preshower.

2 Mean current estimation

The mean current on each anode of the Multi-Anode PhotoMultiplier tubes can be obtained through the following relation :

$$\bar{I}_{(\text{Ampere})} = \bar{Q}_{(\text{Coulomb/MeV})} * \bar{E}_{(\text{MeV/Event})} * \bar{\mathcal{F}}_e(\text{Event/second})$$

where

- $\bar{\mathcal{F}}_e(\text{Event/second})$ is the average event frequency.
- $\bar{E}_{(\text{MeV/Event})}$ is the mean energy deposit in scintillator tile per event.
- $\bar{Q}_{(\text{Coulomb/MeV})}$ is the total charge on the corresponding MA-PMT anode per unit of energy deposit.

The product $\bar{E}_{(\text{MeV/Event})}\bar{\mathcal{F}}_e(\text{Event/second})$ does not depend on the "event" definition. However the following convention has been adopted. An "event" is a bunch-bunch collision with one or more "interaction(s)" where an "interaction" has to be understood as a single proton-proton interaction. RAWH2 samples of simulated p-p collisions then provide "events" corresponding to the mean instantaneous luminosity at LHCb collision point : $\bar{\mathcal{L}} = 2.10^5 \text{ mb}^{-1} \text{ s}^{-1}$ [2].

2.1 $\bar{\mathcal{F}}_e$: the event frequency

The mean event frequency can be obtained as :

$$\bar{\mathcal{F}}_e = \mathcal{R}\bar{\mathcal{F}}_b$$

where $\bar{\mathcal{F}}_b$ is the mean bunch-crossing frequency and \mathcal{R} the ratio of interacting bunch-crossings (i.e. "events").

- Due to the displaced LHCb interaction point and LHC beam structure, 73.57% of bucket crossings involve non-empty proton bunches. With a 40.08 MHz nominal buckets frequency, the effective bunch-crossing frequency is [4] :

$$\bar{\mathcal{F}}_b = 0.7357 * 40.08 = 29.49 \text{ MHz}$$

- Poissonian law provides the fraction of interacting bunch-crossing (i.e. "events") as $\mathcal{R} = \mathcal{P}(n > 0, \bar{\nu}_b) = 1 - e^{-\bar{\nu}_b}$. The mean number of "interactions" per bunch-crossing, $\bar{\nu}_b$, can be obtained as the ratio of the mean interaction frequency $\bar{\mathcal{F}}_i$ and the above described bunch-crossing frequency $\bar{\mathcal{F}}_b$. The interaction frequency $\bar{\mathcal{F}}_i$ is :

$$\bar{\mathcal{F}}_i = \sigma_{pp}\mathcal{L} = 20.48 \text{ MHz}$$

with the generic proton-proton cross-section $\sigma_{pp} = 102.4 \text{ mb}$ [4] and $\bar{\mathcal{L}} = 2.10^5 \text{ mb}^{-1} \text{ s}^{-1}$. The average number of interactions per bunch-crossing is then :

$$\bar{\nu}_b = \bar{\mathcal{F}}_i / \bar{\mathcal{F}}_b = 0.694$$

and the fraction of interacting bunch-crossings :

$$\mathcal{R} = \mathcal{P}(n > 0, \bar{\nu}_b) = 1 - e^{-\bar{\nu}_b} = 50.04\%$$

Finally, the event frequency is :

$$\bar{\mathcal{F}}_e = \mathcal{R}\bar{\mathcal{F}}_b = \mathbf{14.75 \text{ MHz}}$$

with a mean number of interactions per event of :

$$\bar{\nu}_e = \frac{\bar{\mathcal{F}}_b}{\bar{\mathcal{F}}_e} \bar{\nu}_b = 1.388$$

Obviously, the same event frequency value holds for both PS and SPD .

2.2 \bar{E} : the energy deposit

The estimation of the energy deposits in SPD and PS is based on a large RAWH2 sample of simulated minimum bias events. Such simulated events match with the above adopted "event" definition corresponding to an instantaneous luminosity of $\bar{\mathcal{L}} = 2.10^5 \text{ mb}^{-1} \text{ s}^{-1}$. Generated events are reconstructed using the LHCb-light geometry from v248r4 database.

In order to reduce the memory usage in run time and disk spaces, thresholds on energy deposit are applied at the GEANT level. In addition delta rays, beam-gas halo, particles from LHC tunnel ... are not implemented in the standard simulation. All that could lead to an underestimation of the energy deposits. However, it has been checked within the old geometry reconstruction (LHCb classic database v245r1), that the mean PS and SPD energy deposits from special Monte-Carlo production, using lowered GEANT thresholds, delta rays and GCALOR interface for better neutrons simulation, are not significantly different from the corresponding standard simulation.

The distribution of the energy deposit accumulated for all channels, is shown on Fig. 1 for PS and SPD respectively. With an occupancy rate close to 20% (i.e. zero deposit for 80% of events) the total energy deposit in hottest PS channel is almost equally shared between minimum of ionisation deposits (around 3 MeV in 1.5 cm of plastic scintillator) and larger deposits up to 300 MeV from showers in PS lead.

As expected the SPD energy is dominated by Minimum Ionising Particles (MIP) deposits although larger deposits from showers in the material in front of calorimeter system also contribute.

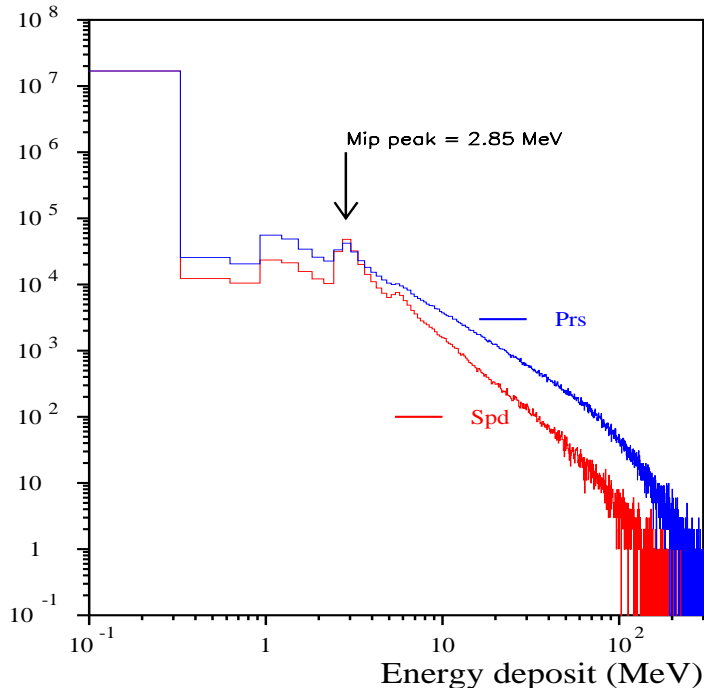


Figure 1: Distribution of the SPD and PS energy deposit accumulated over the 5952 scintillator tiles. The accumulation at 2.85 MeV corresponds to the peak of minimum of ionisation deposit. A second peak corresponding to 2 Minimum Ionising Particles deposit can also be seen. The drop below 1 MeV is an effect of the thresholds at the GEANT level in simulation. It has been checked to not significantly affect the average energy deposit.

Fig. 2 display a 3D representation of the mean energy deposit in each of the PS and SPD scintillator cells. Averaged over the whole scintillator planes, the mean energy deposit is 0.22 MeV/Event/Channel and 0.07 MeV/Event/Channel for PS and SPD respectively. It reaches 2.0 MeV/Event and 0.5 MeV/Event respectively for the hottest channel located in the inner PS region close to the beam pipe.

Clear disymmetries due to the magnetic field can be observed on Fig. 2, meaning that a large fraction of the energy deposit is due to charged particles. More details about the origin of the deposits in the hottest PS and SPD channels are reported in tables 1 and 2 respectively. Homogeneously over the whole preshower, more than 50% of the energy deposits in each PS tile originate from electromagnetic interacting particles : electrons ($\sim 30\%$ of the mean deposit) and photons ($\sim 25\%$). Charged hadrons contribute for almost 45%, essentially π^\pm ($\sim 35\%$), protons and K^\pm ($\sim 3.5\%$ each). A certain fraction of hadrons interacts in the PS lead, leading to a mean energy deposit of ~ 8 MeV/hit.

On the contrary, 65% of the SPD energy originate from charged hadrons : π^\pm ($\sim 50\%$), protons ($\sim 8\%$) and K^\pm ($\sim 6\%$), that essentially interact at the minimum of ionisation, leading to a mean deposit of 4.6 MeV/hit slightly above the mean MIP value (i.e. 3.2 MeV per muon hit). Electrons also contribute as Minimum Ionising Particle for 30% of the mean SPD deposit.

Note that the Monte-Carlo particle type assigned to an energy deposit is submitted to the simulation rules, and MC-particles identity does not always match the actual produced particle. This is

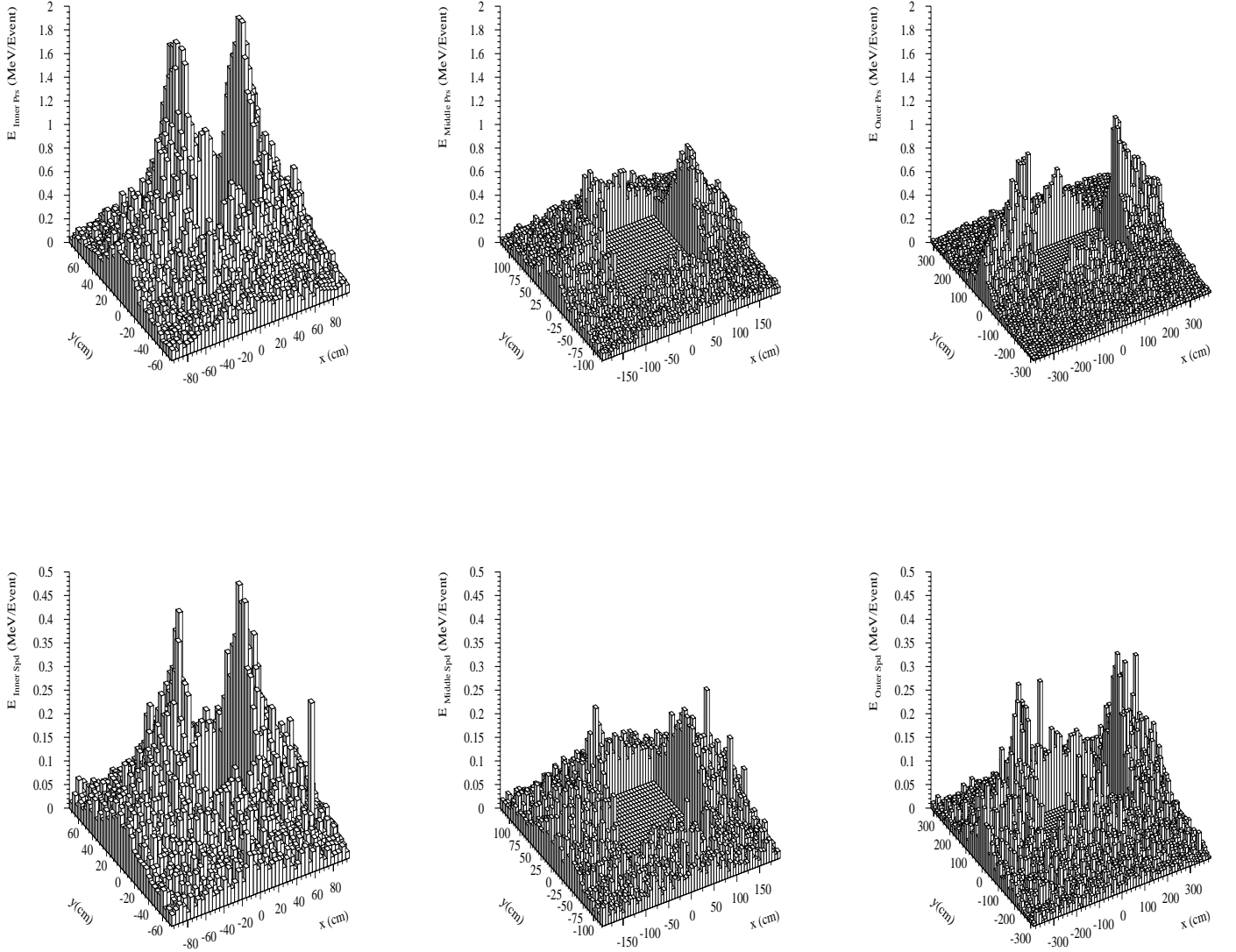


Figure 2: Energy deposit (MeV) in each of the 5952 Ps (top) and SPD (bottom) scintillator tiles for the three cell size regions (inner to outer from left to right).

the case in particular when radiative processes are involved. As example radiated photons are not always distinguished from primary electrons, while photons from π^0 decay are always MC identified. In regard to this restriction, tables 1 and 2 and Fig. 3 have to be understood as a rough indication of the origin of deposits.

While deposits from neutral and charged hadrons essentially originate from the collision point, a large fraction of electrons is due to conversion in the detector material in front of the calorimeter system, as can be seen on Fig. 3. Eventually, a small fraction of deposits (0.2% in Ps and 2% in SPD) is due to backplash particles from ECAL (and/or Ps for SPD) essentially driven by pions, protons and light nuclei (deuteron, triton, alpha).

In the following, the mean energy deposits per event from Fig. 2 is assumed for the mean current estimation in each channel.

particle type	occupancy (hits/10 ³ events)	mean deposit (MeV/hit)	mean energy (keV/Event)	relative deposit (%)
e^\pm	77	8.2	633	32.3
γ	42	11.3	474	24.2
electromagnetic	119	9.3	1.11 MeV/Event	56.5
π^\pm	87	7.7	670	34.2
p	8	8.3	66	3.4
K^\pm	8	8.5	68	3.5
others	0.2	9.1	2	0.1
charged hadrons	103	7.8	0.81 MeV/Event	41.2
n	3	7.6	20	1.2
K_L°	2	10.4	20	0.9
others	0.3	5.1	2	0.1
neutral hadrons	5	7.5	0.04 MeV/Event	2.2
μ^\pm	0.8	3.2	3	0.1
Total	228	8.6	1.96 MeV/Event	100

Table 1: Various particles contribution to the energy deposit in the hottest PS scintillator cell. The particle type refers to the particle at the entrance of the preshower system, in particular before a possible conversions in lead. The first two columns are listing the hit contribution in term of occupancy (hits/event) and mean deposit (Mev/hit). Note that the corresponding values are relative to the thresholds applied at the level of the particle generation. The last two columns are listing the global contributions (keV/Event, that can also be obtained as the product of the two previous columns) and the relative contribution with respect to total of contributions. The "other charged hadrons" row sums the contributions of Σ^\pm , Ξ^\pm as well as light nuclei (deuton, triton and alpha). The "other neutral hadrons" row sums the contributions of K_S° , Λ° and Ξ° .

particle type	occupancy (hits/10 ³ events)	mean deposit (MeV/hit)	mean deposit (keV/Event)	relative deposit (%)
e^\pm	43	3.1	135	30.8
γ	4	2.3	10	2.2
electromagnetic	47	3.1	0.15 MeV/Event	33.0
π^\pm	51	4.3	220	50.0
p	6	6.2	35	7.9
K^\pm	5	5.6	25	5.7
others	0.2	15.2	3	0.6
charged hadrons	62	4.6	0.28 MeV/Event	64.2
n	1	4.1	5	1.1
K_L°	1	6.0	5	1.1
others	0.03	3.0	0.1	0.02
neutral hadrons	2	5	0.01 MeV/Event	2.2
μ^\pm	0.8	3.2	3	0.6
Total	111	4.0	0.44 MeV/Event	100

Table 2: Same as table 1 for the hottest SPD cell.

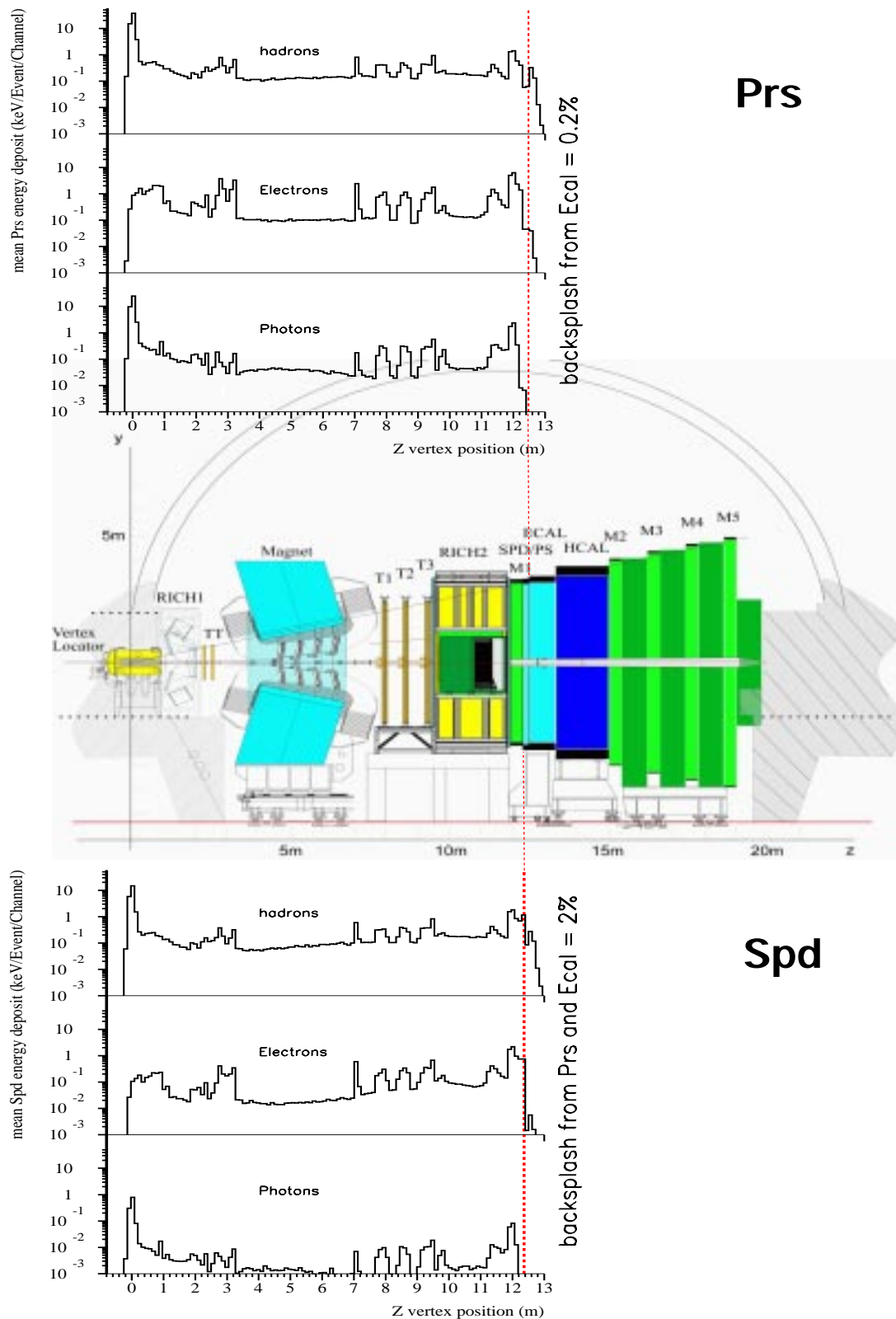


Figure 3: Distribution of the originating vertex position along the beam axis (cm) weighted by the mean energy deposit (keV/Event/Channel) in Prs (top) and SPD (bottom) scintillators for charged hadrons, electrons and photons ($\sim 97\%$ of the total energy deposit).

2.3 \bar{Q} : the anodic charge per MeV deposit

Each MeV deposit within a scintillator tile is converted to an electrical charge directly proportional to the gain of the corresponding MA-PMT channel and to the number of produced photoelectrons :

$$\bar{Q}_i \text{ (Coulomb/MeV)} = G_i * N_i \text{ (p.e./MeV)} * 1.6 \cdot 10^{-19} \text{ (Coulomb/p.e.)}$$

where N_i is the number of photoelectrons per MeV deposit and G_i the photomultiplier gain for the i^{th} readout channel.

The PMT voltage will be adjusted in order to ensure that the overall gains fulfill the requirements for the PS or SPD Very Front-End dynamics. Because both PS and SPD readout dynamics are defined with respect to Minimum Ionising Particle deposit, it is more convenient to use an energy deposit unit, hereafter called *mip* (to be distinguished from MIP the Minimum Ionising Particle), based on the minimum of ionisation in scintillator tile.

In addition, since the gain choice depends on the Front-End readout designs, it is convenient to estimate the anodic charge from the electronics point of view as :

$$\bar{Q}_i \text{ (Coulomb/MeV)} = \bar{Q}_{ref} \text{ (Coulomb/mip)} * R_{(mip/MeV)} * \frac{g_i}{g_{ref}}$$

where

- \bar{Q}_{ref} is the anodic charge for a reference channel and for the reference deposit (*mip*) as defined from electronics design. The estimation of the charge \bar{Q}_{ref} per *mip* is addressed in subsections 2.3.2 and 2.3.3 for PS and SPD respectively.
- R is the *mip* to MeV conversion factor. The MIP energy deposit is Landau distributed. Hence, the maximum of distribution does not coincide with the mean deposit. This leads to some ambiguities in the *mip* definition. It has been chosen to define the *mip* unit from the peak position of the distribution of the energy deposit by MIP, that is : $R = (2.85 \text{ mip/MeV})^{-1}$. It means that MA-PMTs gain have to be calibrated accordingly, i.e. with respect to the peak of MIP deposit. This is a conservative (maximizing) definition in term of charge with respect to the mean MIP deposit which is about 15% larger than the peak.
- g_i/g_{ref} is the relative gain of i^{th} channel with respect to the reference one. This gain ratio is discussed in subsection 2.3.1

2.3.1 Gain non-uniformities

MA-PMT handles 64 channels sharing the same voltage supply. The intrinsic gain non-uniformities within MA-PMT is non adjustable. The gain will then vary with the amplification chain i .

The gains of one R-5900 64A-PMT has been scanned using constant light yield. As shown on Fig. 4 a 1:2 non-uniformity between anodes is observed. The overall relative gain is 1.4.

Assuming a non-uniformity as large as 1:2, the gain mapping of Fig. 4(left) is adopted and duplicated for all MA-PMTs within the standard VFE-Board mapping design [3] shown on Fig. 5.

In addition, the light yield dispersion between channels has been included as an additional source of non-uniformities. This is performed with a random full gaussian smearing of gains with a width of $\sigma = 15\%$, as observed in test-beam study of PS /SPD module [5]. The lowest gain channel of each MA-PMT is defined according to the overall non-uniformity (combining PMT amplification

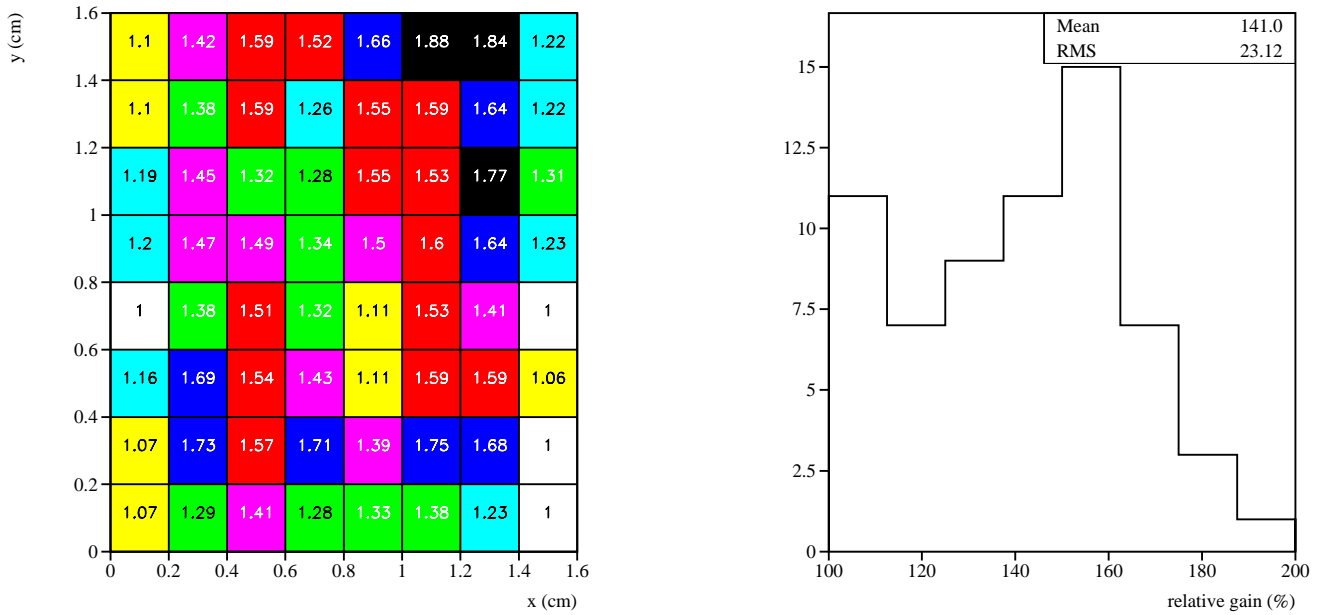


Figure 4: Relative gain mapping (left) and distribution (right) for the 64 anodes of R-5900 64A-PMT. The relative gain over MA-PMT is 1.4 on average.

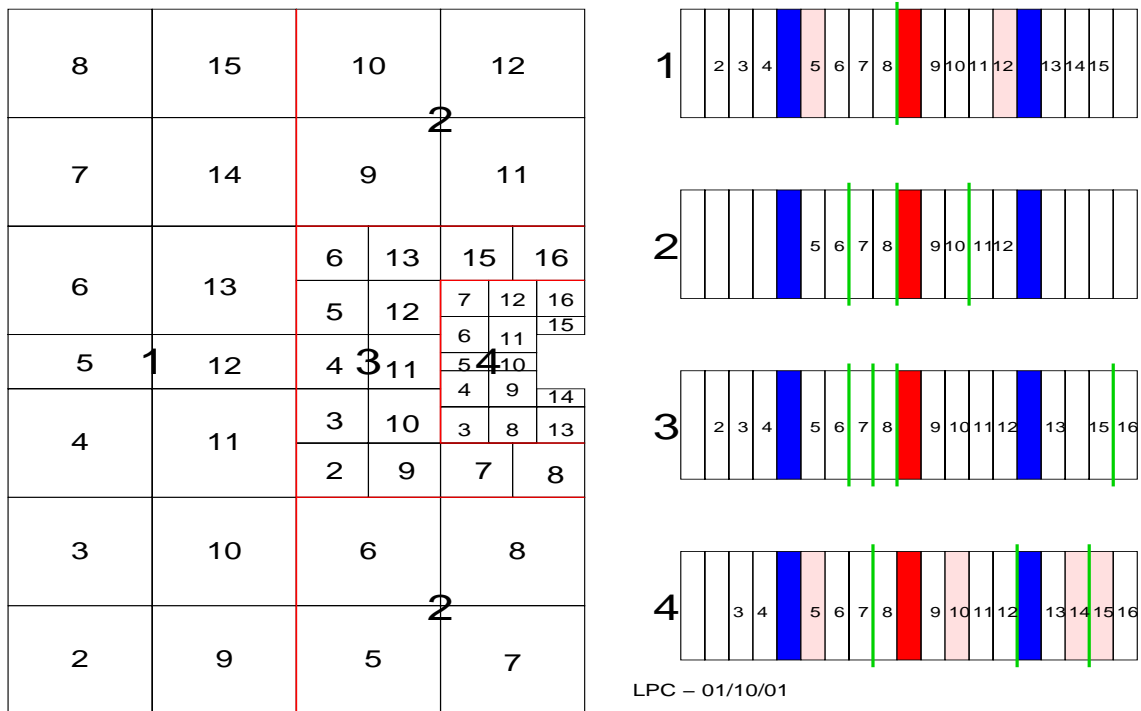


Figure 5: MA-PMT and VFE-Board mapping [3].

and light yield) that ranges in the 1:4 ratio with a 1.8 average value.

It is worth noticing that the charge per mip is very sensitive to the overall non-uniformity range due to its scaling with respect to the lowest gain. A large non-uniformity ratio implies large charge per mip for large gain channels. A quality selection of both MA-PMT and modules according to

small non-uniformities will help reducing the average anode charge. Accordingly, the gaussian light yield dispersion with $\sigma = 15\%$ that has been adopted here, could be pessimistic assuming that a selection of module will restrict the photostatistics dispersion in a smaller range.

As an exemple, the overall non-uniformity would range in the 1:2.5 ratio with an average value of 1.6 when the light yield dispersion were limited to an absolute range of $\pm 15\%$ (from the minimal to the maximal value within each MA-PMT). This $\pm 1\sigma$ allowed range would however imply the rejection of one third of the cells. Because light yield non-uniformity is likely due to connector when the 16-cells modules are mounted this selection would imply the rejection of almost all the modules !! It is then very important to foresee the reduction of the RMS of the light yield dispersion to a value as small as possible before the mass production of modules. Assuming that a dispersion of $1\sigma = 5\%$ could be reached (e.g, 20 ± 1 photoelectrons), the $\pm 15\%$ allowed range would correspond to 3σ and then lead to the rejection of almost 0.3% of the cells and consequently to the more reasonable rate of 5% of the modules.

2.3.2 Anodic charge \bar{Q}_{ref}^{Ps} for Ps

The preshower tasks require a 10 bits dynamics with a *mip* /10 Least Significant Bit precision [6]. While the Level-0 pipeline of Front-End electronics is clocked at 40 MHz, the PS pulse duration is larger than 25 ns. The *mip* definition for the preshower electronics engineers is then simply : a 10 ADC counts signal in the highest of successive 25 ns samplings. The integration clock could possibly be shifted in order to maximize the signal fraction in the main 25 ns sample. The electronics *mip* definition, and then the corresponding anodic charge, thus slightly depends on the shape and timing of the MA-PMT pulse.

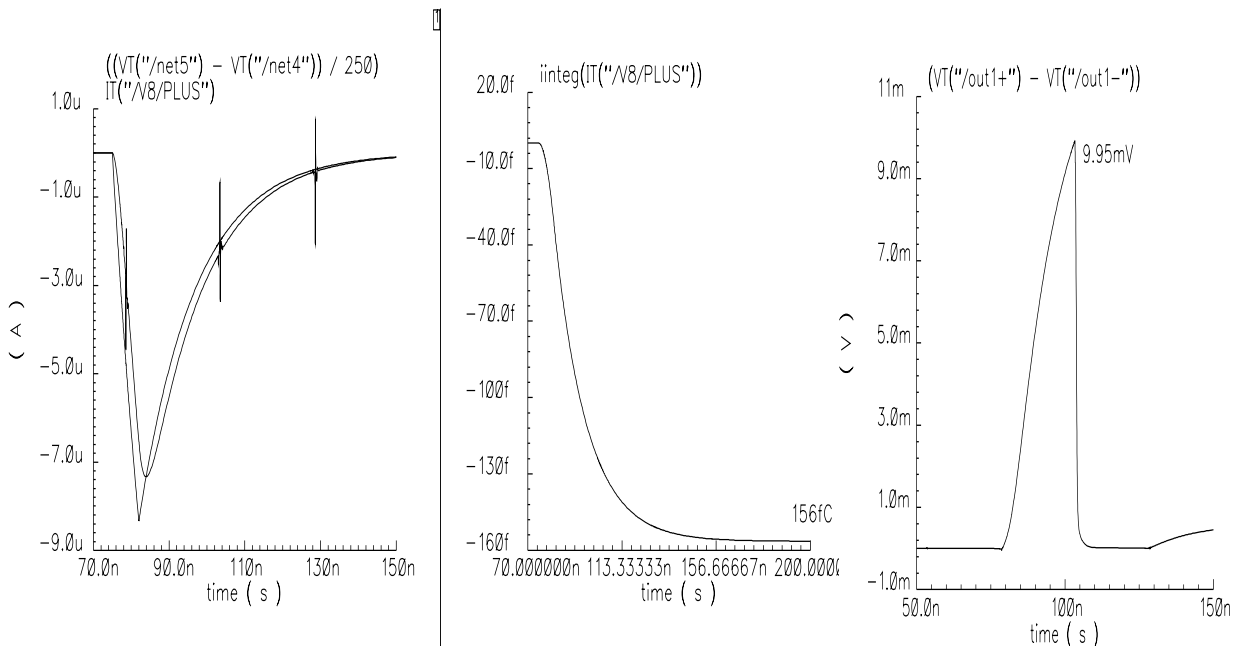


Figure 6: *Left* : generated MA-PMT signals (μA) with and without the 250Ω load. *Center* : signal integrations (fC). Total integrated charge is 156 fC. *Right* : signal after integrator (mV). The electronics design ensures the same value to be reached at the ADC level. Maximal tension is 9.95 mV corresponding to 1% of the 1 V ADC dynamics, i.e. 10 ADC counts for 10 bits dynamics.

The MA-PMT gain for preshower will therefore be calibrated in such a way that the *mip* corresponds to 10 ADC counts for a reference channel. The reference channel among the 64 handled by a Front-End board is the one of lowest gain, the gains uniformity being restored by decreasing the electronics

gain in the readout chain for the other channels. In the current readout design the gains are standardized using load resistors, with a maximal resistance value of 250Ω assigned to the reference channel.

A simulation of the current design of the electronics readout chain has been applied to extract the anodic charge for the *mip* signal adjusted to 10 ADC counts as discussed above. The input signal is a simulated typical *mip* current pulse (4 ns triangular rising front followed by 13 ns exponential decay, $RC=1.8$ ns). The resulting integrated charge is $\bar{Q}_{ref}^{PS} = 156 \text{ fC}/mip$ as summarized on Fig. 6.

In the following the value :

$$\bar{Q}_{ref}^{PS} = 160 \text{ fC}/mip$$

is assumed as the reference charge for the Ps MA-PMT channel of lowest gain. Assuming a typical amount of 20 photoelectrons per *mip* [5] this corresponds to a MA-PMT gain $G_{ref} = \mathcal{O}(5 \cdot 10^4)$. Including gain non-uniformities (1.8 on average), the averaged charge over channels is $290 \text{ fC}/mip$.

2.3.3 Anodic charge \bar{Q}_{ref} for SPD

In order to avoid a fast MA-PMT ageing the SPD readout is requiring a maximal charge per *mip* deposit of :

$$\bar{Q}_{ref}^{SPD} = 100 \text{ fC}/mip$$

So the MA-PMT voltage will be adjusted in such a way that the SPD reference channels, defined as the largest gain one, will receive 100 fC on average with a *mip* deposit. As for Ps, this charge is accounted all along the MIP pulse, not only in a 25 ns window. Taking the gain non-uniformities into account, the averaged charge over channels is then about $60 \text{ fC}/mip$, that is a factor 5 lower than for Ps. The maximal charge corresponds to reference gain of $G_{ref} = \mathcal{O}(3 \cdot 10^4)$ for a typical amount of 20 photoelectrons per *mip*.

The SPD dynamics requires in addition the resolution of the discriminator to be better than 0.1 *mip* for all channels, in order to keep the energy resolution given by the photostatistics in the 0.7 *mip* threshold area [7]. From preliminary measurements based on MIP signal, the signal-to-noise ratio is around 40 for a 100 fC signal charge when using a 400Ω MA-PMT load resistor. The 1:2 ratio for MA-PMT non-uniformities is then covered with a signal-to-noise ratio larger than 20 for all channels. Therefore, it still remains a certain margin to compensate for additional non-uniformities from light or for noise increases in the final environment. In addition the signal-to-noise ratio may be furthermore increased with a larger MA-PMT load resistance value.

2.4 \bar{I} : the mean anodic current

All ingredients needed for the estimation of the mean anodic PS and SPD currents are summarized below :

- The event frequency $\bar{\mathcal{F}}_e = 14.75 \text{ MHz}$ for both PS and SPD .
- The mean event deposit $\bar{E}_{(MeV/Event)}$ for each of the PS and SPD channel, from Fig. 2.
- The reference anodic charge $\bar{Q}_{ref}^{PS} = 160 \text{ fC}/mip$ and $\bar{Q}_{ref}^{SPD} = 100 \text{ fC}/mip$.
- The MA-PMT gain non-uniformities from Fig. 4 convoluted with 15% light yield non-uniformity.
- The *mip* to MeV conversion factor : $1 \text{ MeV} = 2.85 \text{ mip}$.

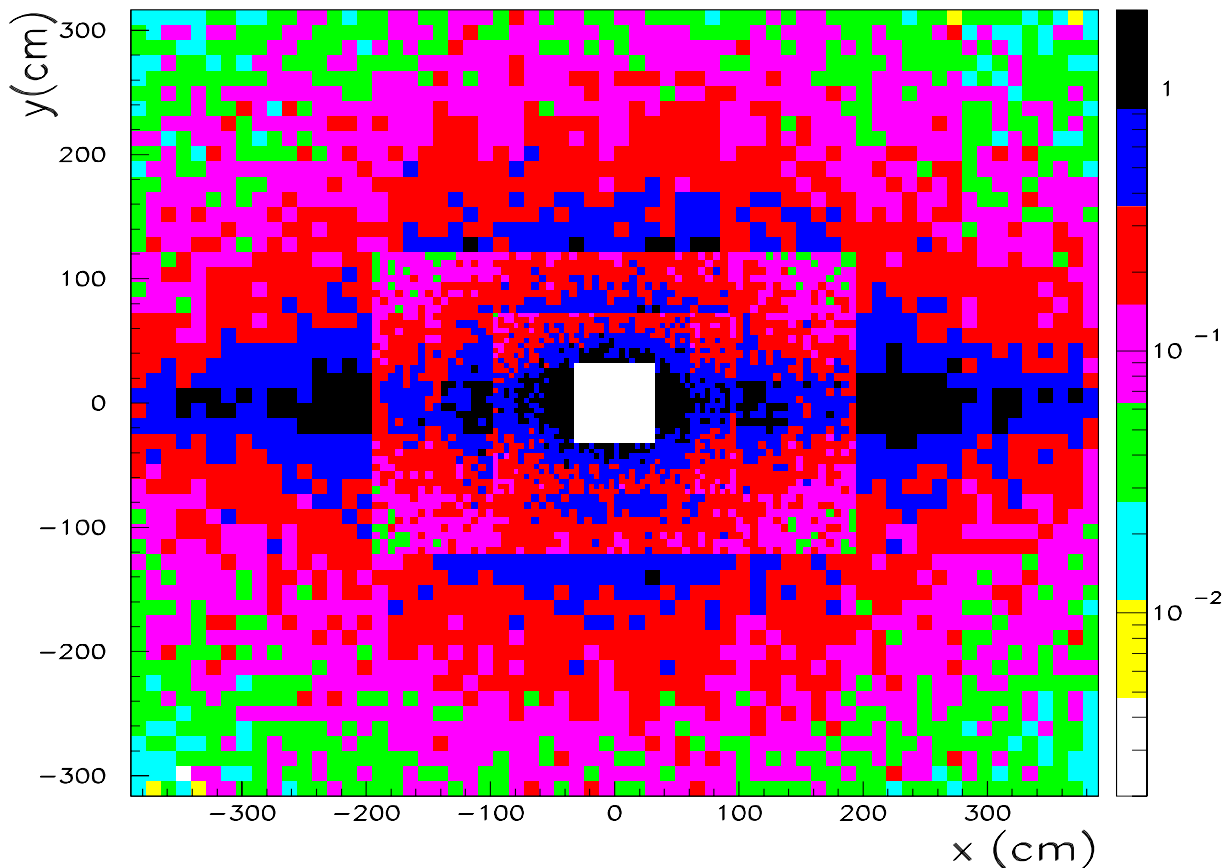


Figure 7: Mean current (μA) in each Ps channel.

The resulting mean PS currents are displayed in Fig. 7 and 8 for each channel and MA-PMT respectively. The maximal current reaches $3.5 \mu A$ in the hottest channel and $0.3 \mu A$ on average over Ps .

The total MA-PMT anodic current exceeds $60 \mu A$ in hottest region. In addition, the luminosity is not constant over a fill and exponentially decreases ($\tau \sim 10 \text{ hours}$) during the fill duration ($\sim 7 \text{ hours}$). The mean instantaneous luminosity $2 \cdot 10^5 \text{ mb}^{-1} \text{ s}^{-1}$ thus leads to a maximal luminosity : $\sim 2.8 \cdot 10^5 \text{ mb}^{-1} \text{ s}^{-1}$. The current is then larger by a factor 1.4 at the beginning of a fill and decays from $100 \mu A$ to $50 \mu A$ for the hottest MA-PMT during the fill life time. These values are far above the base constructor specifications, that could support a $18 \mu A$ maximal current. Most of the MA-PMT in each calorimetric region exceed this limitation.

Moreover, such large currents correspond to a mean charge of $\sim 5 \text{ Coulomb}$ per day for the hottest PS MA-PMTs, leading to a fast depletion of the last dynodes of the amplification chain. Eventually the large asymmetries up to a factor ~ 10 in anodic currents within MA-PMT lead to a non uniform gains ageing between channels that could not be adjustable with HV retuning. Fig. 8(right) displays the current asymmetries for each of the PS MA-PMT.

Due to the lower occupancy and the smaller assumed charge per mip, the situation is much less critical for SPD . The estimated currents for SPD are lower by a factor ~ 15 than PS currents. Hence, the hottest SPD channel withstands $0.2 \mu A$ and the MA-PMT total current reaches $4 \mu A$ at maximum (i.e. 0.3 Coulomb per day) as shown on Fig. 9,

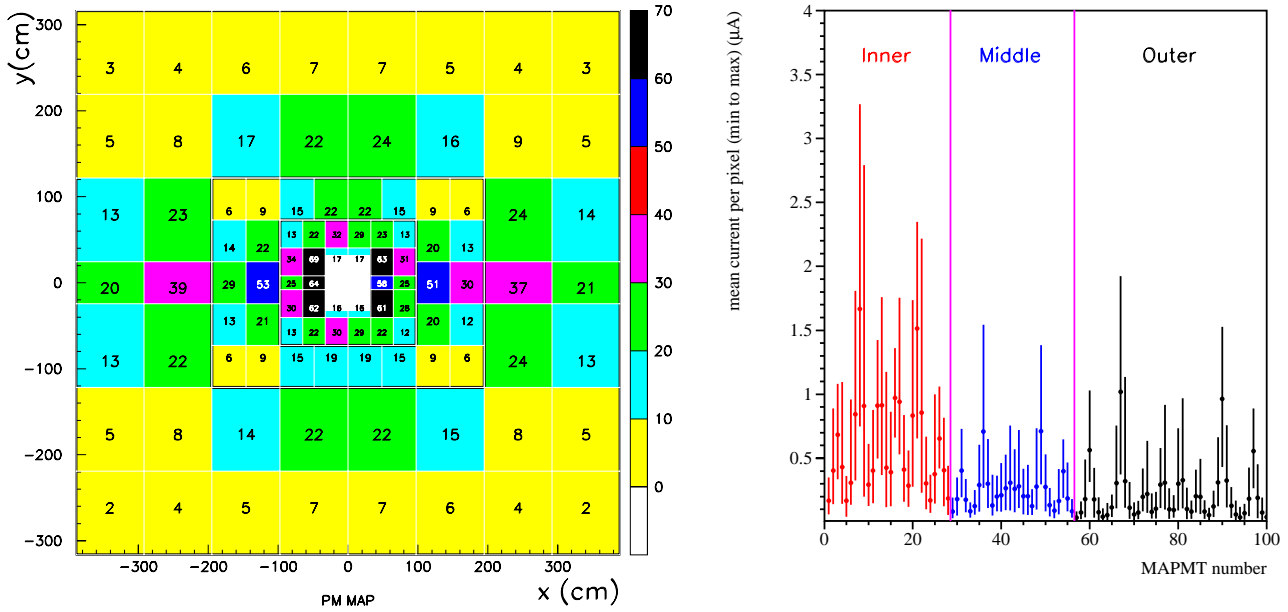


Figure 8: *Left* : Total current (summed over all channels) for each MA-PMT. *Right* : current asymmetries within each of the 100 Ps MA-PMT. Each point corresponds to a single MA-PMT (abscissa is an arbitrary MA-PMT numbering value). Points value and corresponding error bars respectively indicate the mean current and the range from the minimal to the maximal current per channel inside the considered MA-PMT.

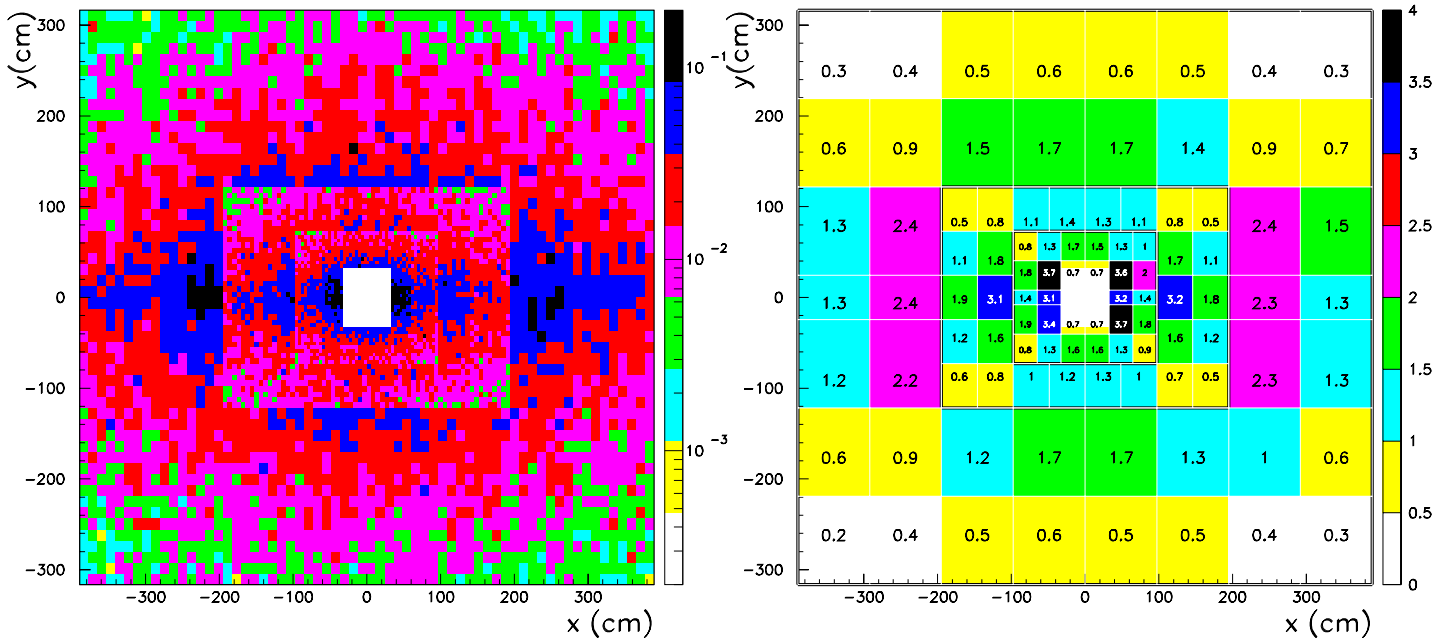


Figure 9: Mean SPD current (μA) in each channel (left) and summed over each MA-PMT (right).

This mean current estimations have now to be compared with experimental ageing test described in the following section.

3 Ageing test bench results

Very few information are available as far as the ageing of the 64A-PMT is concerned. In particular, the measurements given by the constructor are performed by illuminating uniformly the MA-PMT and by connecting all the anodes together. The fibre connection used in both the SPD and PS may change significantly the results because of the amplification sub-structure of the channels. Furthermore, one might want to test the hypothesis of a possible gain recovery in the running conditions of LHCb.

3.1 The experimental setup

The sketch of the test bench is shown Fig. 10. The monitoring of the light system and the data acquisition is performed with an electronics board controlling the input/output from the parallel port of a PC. The commands are written in Labview.

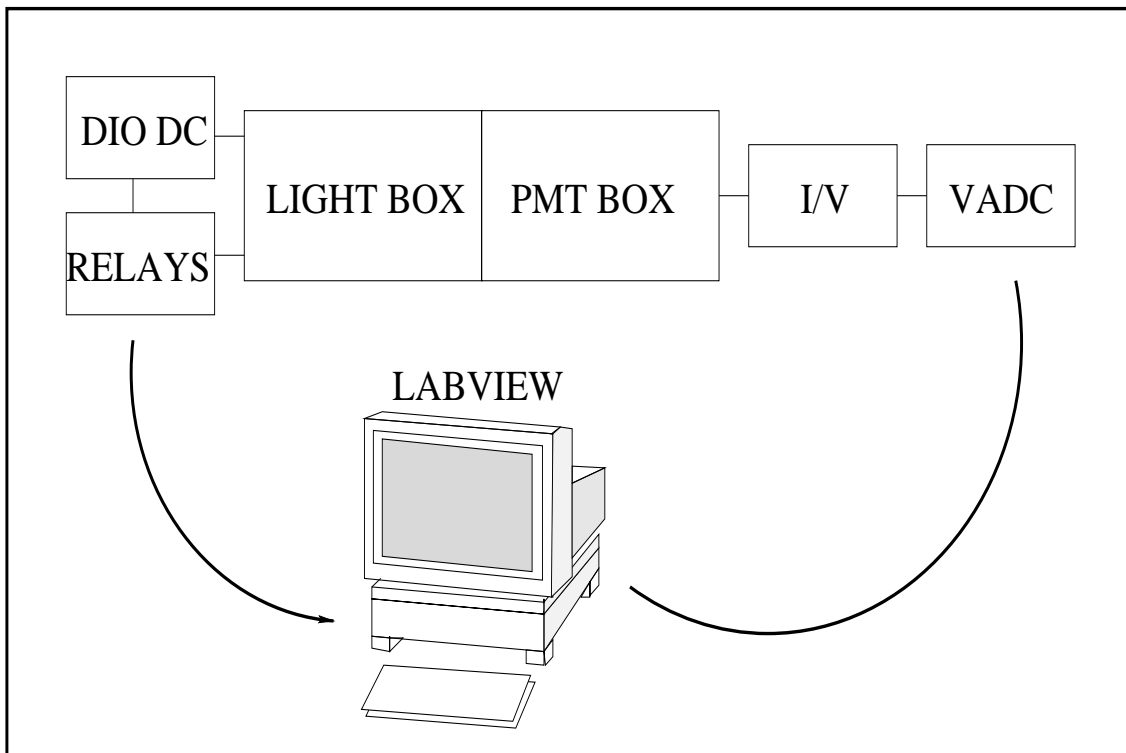


Figure 10: Sketch of the experimental setup of the ageing test bench.

The light system is composed of blue LEDs monitored by relays to operate the MA-PMT channels under intermittent illuminations. Five channels have been instrumented, the light being conducted to the MA-PMT window with a 1mm diameter clear fibre. One channel was continuously illuminated, the four others received an intermittent illumination (one hour light, 3 hours stop). The light yield given by the blue LED has been checked to be stable along the duration of the tests.

The DC voltage supply of the LEDs was set to give a $4 \mu\text{A}$ signal for each anode. In such conditions, the overall average anode current is at the level of the maximal value specified by the constructor and close to the value estimated for the hottest PS channel in the section 2.4.

The acquisition of the MA-PMT signals is performed by a 10 bits voltage ADC -included in the PPIO board and monitored with Labview- after a current/voltage conversion.

3.2 The results

Figure 11 shows the current response of the MA-PMT channel continuously illuminated as a function of the time. A sharp exponential decrease is observed in the first part of the distribution. The physical explanation is related to the structure of the metal dynode channels : the Cs layer in excess is continuously depleted and then do not contribute to the secondary electrons emission. Once this layer is fully depleted, a less violent decrease of the gain (that can be considered linear along the duration of the test) is observed.

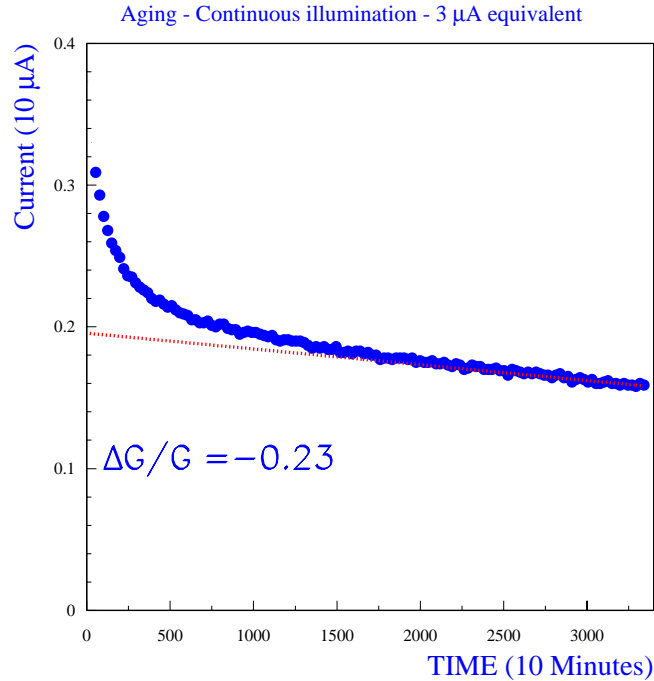


Figure 11: Distribution of the MA-PMT output as a function of the operation time for a continuous illumination.

The same qualitative behaviour has been observed, as shown Fig. 12, for the four other channels, intermittently illuminated. The quantitative responses of these anodes are however not the same. There is no gain recovery in the periods of light stop.

The hypotheses of a gain recovery in absence of a light stress on one hand and after a period of rest on the other hand have been tested. As shown Fig. 12, no significant gain recovery is observed in absence of light stress. On the contrary, it has been observed that after a period of rest of one week, some recovery was achieved despite the usual sharp drop as shown Fig. 13. After one week of operation, the anode current has been measured at its level before the stop. This last result deserves a more accurate scrutiny.

The MA-PMT has been further studied after its ageing using the generic test bench in Clermont that confirms the results in term of gain decrease. Fig. 14 shows the responses of the 64 anodes; the five anodes submitted to the light stress are circled.

3.3 Extrapolation to one LHCb year

To figure out how many MA-PMTs are concerned by significant gain drops for how many channels, a delicate extrapolation exercise was led under the following assumptions : first, the exponential drop is assumed to be under control and already realised when the MA-PMT are operated in the

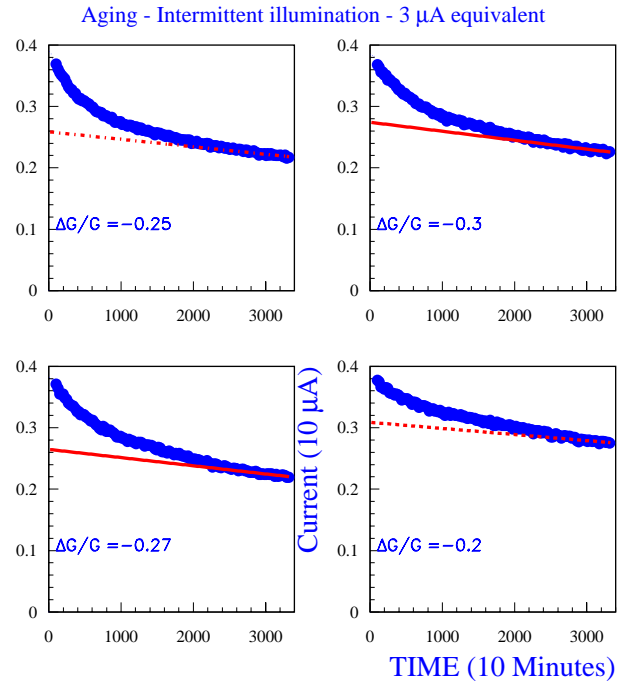


Figure 12: Distribution of the MA-PMT output as a function of the operation time for an intermittent illumination.

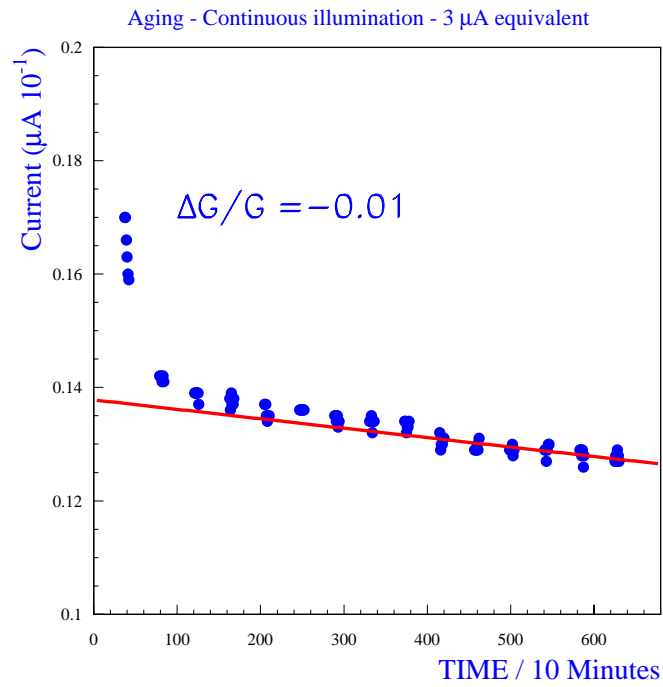


Figure 13: Distribution of the MA-PMT output as a function of the operation time after a period of rest.

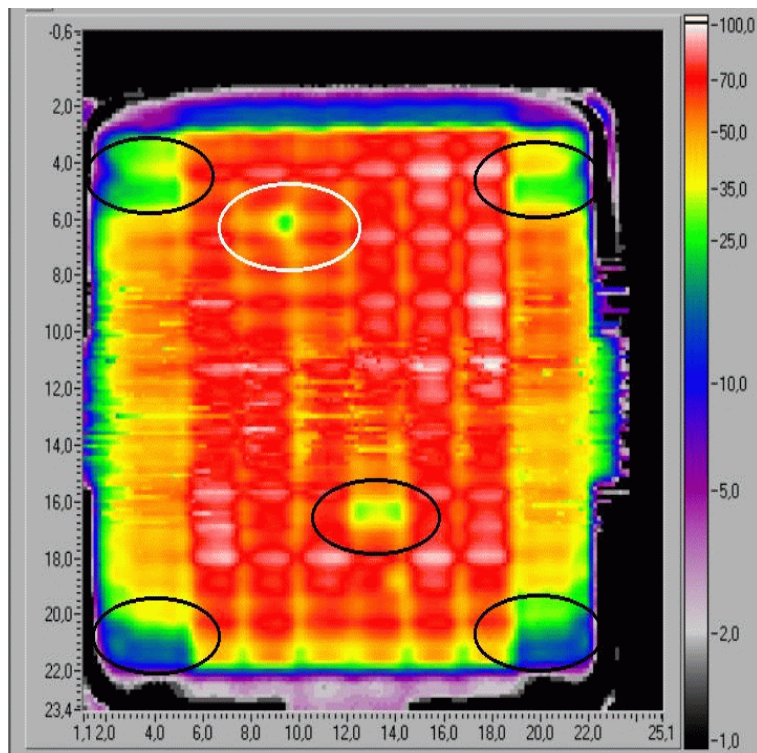


Figure 14: Distribution of the MA-PMT outputs for the 64 anodes after the ageing period. The fired pixels are circled. The white ellipse corresponds to a short test performed with an initial current of $20 \mu A$!

experiment (MA-PMT are aged before the experiment). Second, a typical time acceleration factor as defined by the constructor is considered; this factor states that the ageing is more rapid for a given delivered charge by about 1.5 when the current is lower.

The situations are different for the PS and the SPD, the average anode current being significantly lower in the latter case. As a consequence, only results and estimates for the PS are given in the following.

Fig. 15 shows the number of photomultipliers as a function of their mean gain loss and gains asymmetry for one LHCb year operation. Taking $\pm 25\%$ as the maximal gain correction authorised in the FE electronics, it is observed that a large fraction of the channels are concerned, implying most of the MA-PMT to be degraded.

The same picture was drawn considering ten times less current at the MA-PMT anodes as indicated Fig. 15. The overall picture becomes acceptable.

3.4 VFE electronics solutions

As a consequence of the ageing results, the MA-PMT must be operated at lower voltages. As far as the SPD is concerned, it seems that slight modifications to the VFE board may be sufficient. The gain reduction factor of 10 for the PS seems on the contrary an unavoidable target.

A study has been made to optimize the VFE board of the PS, without modifications to the design. The basic conclusion of this study is that only a reduction of the MA-PMT gain by a factor 2 is possible within the specified performance of the electronics. A redesign of the first stage of the PS VFE board is therefore mandatory to reach the MA-PMT gain reduction of a factor 10. The conception of the new design is now about to be completed (the integrator is almost unchanged) and one channel is going to the foundry beginning of January. The results of the simulation are encouraging, provided that the gain reduction target is reached without degrading the performance

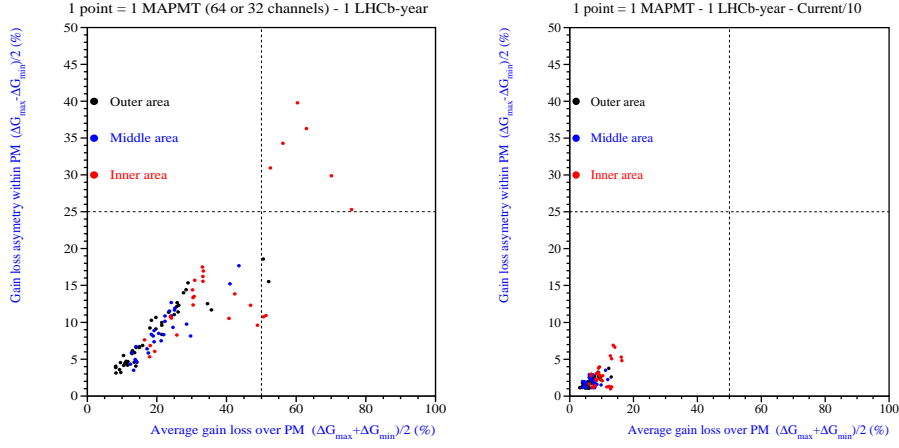


Figure 15: Distribution of the MA-PMTs in term of mean gain loss and gain asymmetry. In the right figure a reduction factor of 10 is assumed for the mean current.

of the electronics chain.

3.5 What if 16A-PMT were used for the hottest channels ?

Due to the fast decrease of the energy deposit when moving away from the beam axis, most of MA-PMT current is located within few channels. Extracting from some of the hottest MA-PMTs the 16 or 2*16 hottest channels to be readout through one or two 16-Anodes PMTs would reduce the maximal MA-PMT current. In addition, the ageing behaviour of 16A-PMT is expected to be less critical than for 64A-PMT due to the factor 4 in dynodes surface.

A MA-PMT mapping including sixteen of 16-Anodes PMTs located in the hottest regions (i.e. at the border of different cell size areas along x direction) is proposed on Fig. 16.

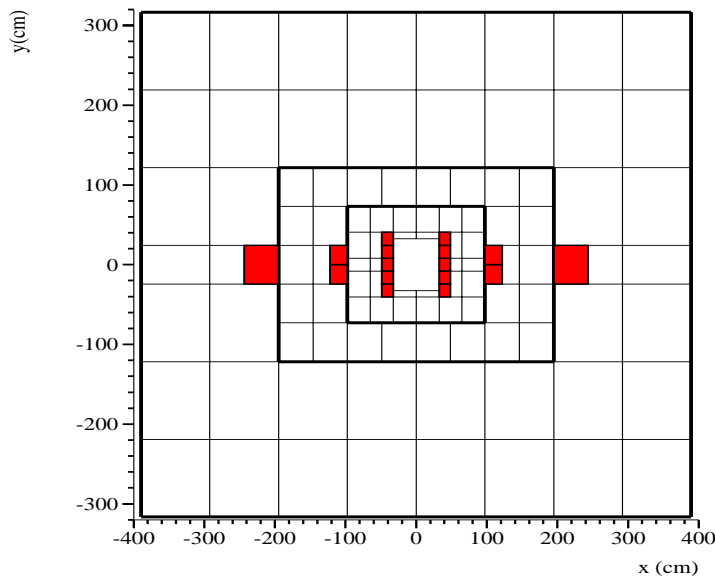


Figure 16: Tentative MA-PMT mapping including 16-Anodes PMTs (shaded areas) in hottest regions.

The obtained MA-PMT current reduction is described in table 3. The hottest MA-PMT now withstands about $30 \mu A$ and $45 \mu A$ for 64A-PMT and 16A-PMT respectively, to be compared to the $65 \mu A$ maximal current in the standard design of 64A-PMT mapping.

Area	VFE-Board Id	total current (μA) within 64A-PMT	total current (μA) shared within 64A-PMT + <i>16A-PMT(s)</i>
Inner	4-09 & 5-09	62	25 + <i>22</i> + <i>15</i>
	4-10 & 5-10	61	21 + <i>44</i>
	4-11 & 5-11	65	28 + <i>19</i> + <i>18</i>
Middle	3-11 & 6-11	52	13 + <i>20</i> + <i>20</i>
Outer	1-12 & 8-12	38	13 + <i>26</i>

Table 3: Current sharing using 16A-PMT for the readout of the hottest channel compared to 64A-PMT current. The bold and italic value in the right column indicates the 64A-PMT and 16A-PMT(s) current respectively. The VFE-Board Id refers to the mapping displayed on figure 5 & to the right side symmetrical boards.

Let us note that the VFE-boards numbered 4-10, 1-2 and their right side symmetricals, only handle 32 channels and could be instrumented with two 16A-PMTs each instead of one 64A-PMT and one 16A-PMT. To the price of adding twenty 16A-PMTs to the hundred 64A-PMT, a potential further reduction of the total anode current by a factor 3 is conservatively reached, e.g a factor 30 including electronics gain improvement.

This solution has to be investigated in regard to the forthcoming results of experimental ageing test to be performed on one hand and to the geometrical constraints of adding 20 photomultipliers to the readout setup.

4 Conclusions, perspectives and time schedule

The choice of the MA-PMT base for both the SPD and PS has been scrutinized in regard to the average anode current, determined from the energy deposits in the detectors in the present design of the VFE electronics.

The results of these studies revealed two main issues : the first one is that the average anode currents for some MA-PMT are beyond the specifications of the constructor, requiring minimally the design of a dedicated base. The second one, far more critical, concerns the ageing of the photodetector. Dedicated studies showed that the gain of the MA-PMT in the conditions of large average anode currents is rapidly decreased and that most of the PS MA-PMT would not survive the very first years of the experiment. The situation is less painful for the SPD . For PS , if a reduction of the average anode current by a factor 10 is considered, it appears that most of the channels are preserved.

Immediate actions are currently underway. First, since the MA-PMT must be operated at lower voltages, the optimal amplification is obtained for the eight dynode stages MA-PMT. Such MA-PMT have been asked for and a dedicated base has been built. With such output currents, the VFE electronics, or at least its first stage must be redesigned. The simulation shows that a reduction factor of 10 seems achievable to the price of a complete redesign of the first stage of the chip. A foundry is expected for the beginning of January.

Simultaneously, a test bench will be set up to measure the response of the MA-PMT under a stress of current decreased by a factor 10. The duration of the test will be six months and the test bench is expected to be in operation at the beginning of January. The very first weeks of the test will give information about the exponential drop. If the results are consistent with a correct

operation of the MA-PMT, the time schedule of the MA-PMT procurement and the production of the electronics will not need to be modified.

Acknowledgements.

PICS and Integrated Action should be acknowledged. PICS agreement is between Generalitat de Catalunya and CNRS. Integrated Action is between spanish and french governments. BCN side should also acknowledge support from CICYT under contract fpa2002-04452-c02.

We also would like to thank Ivan Korolko and Jacques Lefrançois for useful discussions.

References

- [1] *LHCb Calorimeter Technical Design Report*, CERN/LHCC/2000-0036 (2000).
- [2] *LHCb Technical Proposal*, CERN/LHCC 98-4, LHCC/P4 (1998).
- [3] *Cards and crates layout for the calorimeter front-ends electronics*, Callot O., Perret P., LHCb 2002-015 (2002).
- [4] *Event yield*, Schneider O., 22 november 2002 LHCb-light meeting.
- [5] *Preshower testbeam results*, Lefèvre R., 17 september 2002 Calorimeter meeting.
- [6] The mixed analog/digital shaper of the LHCb preshower, Lecoq J., 7th Workshop on Electronics for LHC experiments, Stockholm, Sweden (2001)
- [7] *A BiCMOS Synchronous Pulse Discriminator for the LHCb Calorimeter System*, D. Gascon et al., 8th Workshop on Electronics for LHC experiments, Colmar, France (2002)